Hindawi
International Journal of Polymer Science
Volume 2019, Article ID 2575987, 11 pages
https://doi.org/10.1155/2019/2575987

Research Article

Functionalization of 3D Polylactic Acid Sponge Using Atmospheric Pressure Cold Plasma

G. Gatti,[1,2] **D. D'Angelo**,[3] **M. Errahali**,[1] **M. Biasizzo**,[4] **L. Marchese**,[1,2] **and F. Renò**[5]

[1]*Dipartimento di Scienze e Innovazione Tecnologica, University of Eastern Piedmont, V. Teresa Michel 11, 15121 Alessandria, Italy*
[2]*Nano-SISTEMI Interdisciplinary Centre, Università del Piemonte Orientale A. Avogadro, V. Teresa Michel 11, 15121 Alessandria, Italy*
[3]*Plasma Nano-Tech, Environment Park S.p.A, Via Livorno 60, 10144 Turin, Italy*
[4]*Chemistry Department I.F.M, University of Turin, Via Pietro Giuria 7, 10125 Turin, Italy*
[5]*Innovative Research Laboratory for Wound Healing, Health Sciences Department, University of Eastern Piedmont, Via Solaroli 17, 28100 Novara, Italy*

Correspondence should be addressed to G. Gatti; giorgio.gatti@uniupo.it

Received 28 June 2018; Accepted 15 October 2018; Published 13 February 2019

Academic Editor: Angel Concheiro

The deposition of organic functionalities on biomaterials to immobilize biomolecules is a research area of great interest in the medical field. The surface functionalization of a 3D porous scaffolds of $P_{DL}LA$ with carboxyl (-COOH) and amino ($-NH_2$) groups by cold plasma treatment at atmospheric pressure is described in this paper. Two methods of continuous and pulsed plasma deposition were compared to assess the degree of functionalization of the internal porous 3D scaffold. In particular, the pulsed plasma treatment was found to functionalize uniformly not only the sample surface but also inside the open cavities thanks to its permeability and diffusion in the porous 3D scaffold. The species developed in the plasma were studied by optical emission spectroscopy (OES) technique, while the functionalization of the sponges was evaluated by the Diffuse Reflectance Fourier-Transform Infrared Spectroscopy (DR-FTIR) technique using also the adsorption of ammonia (NH_3) and deuterated water (D_2O) probe molecules. The functional groups were deposited only on the front of the sponge, then the structural characterization of both front and back of the sponge has demonstrated the uniform functionalization of the entire scaffold.

1. Introduction

Polylactic acid is a biodegradable aliphatic polymer existing both as P (L) LA and P (D) LA (hereafter $P_{DL}LA$). $P_{DL}LA$ undergoes scission in the body to lactic acid with L-lactic acid as a natural intermediate in carbohydrate metabolism [1, 2]. Thus, $P_{DL}LA$ is suitable for use in reabsorbable sutures, carriers for drug and growth factor delivery, peripheral nerve guidance channels, vascular devices, and implants for orthopaedic surgery also thanks to its good mechanical property system [3, 4]. Unfortunately, the hydrophobicity and low surface energy of these polymers lead to inefficient cell attachment, spreading, and proliferation [5]. Biologic response to biomaterial implantation is determined by their surface characteristics rather than bulk properties; therefore, a wide range of surface modification methodologies have been used to modify their surface properties in terms of wettability, surface energy, and topography; these characteristics modulate the cellular responses such as cell adhesion or foreign body reaction [6–9].

Every approach aimed at modifying biomaterial surface should be able to introduce physical and/or chemical modifications in the outer molecular layer. Moreover, when attempting to modify a 3D structure, it is essential that the modification process reaches the bulk. In light of these considerations, plasma-driven modifications represent a very interesting tool to reach such objectives [6].

In the last few years, gas plasma treatments have been extensively used to modify biomaterials for tissue engineering applications [10, 11]. In particular, plasma surface activation process employs gases, such as oxygen or argon, which dissociate and react with the surface and used to create

additional functional groups on the surface that can be recognized as adhesion sites for surrounding cells [12–15], whereas N_2 and NH_3 gases should be used for treatments in which it is possible to incorporate both nitrogen-containing groups [16, 17].

As reported in previous paper, plasma grafting (obtained by plasma treatment with gases) is distinct from plasma polymerization because the first graft functional groups are on the polymer surface while the second one coats the substrate with covalently bind thin film. Two of the most efficient monomers used for plasma polymerization and grafting in vacuum on biodegradable polymers are acrylic acid (AA) and 1,2-diaminopropane (DAP) [18, 19]. Polylactide polymers do not contain functional groups with enhanced surface hydrophilicity: the presence of carboxylic and amine groups thus enhances the adhesion of epithelial cells [20, 21], representing optimal candidates for gas plasma surface modification [22–25].

In a previous study [26], our group obtained good results by modification of PLA film surface using an atmospheric pressure plasma treatment. These promising results fostered further studies in order to increase the biocompatibility of 3D structures [27]. In the present study, we produced a 3D PLA sponge in order to create a biodegradable scaffold that could potentially be used for biomedical application such as bone reconstruction and tissue regeneration.

In particular, the surface modification was obtained by applying two different plasma processes: a first one based on continuous plasma and a second one based on pulsed plasma treatment. Such dual technical approach has been chosen in order to evaluate plasma penetration in the 3D framework.

It is known that during plasma polymerization monomers may undergo considerable decomposition or fragmentation of chemical functions, resulting in the formation of radicals that can participate in the plasma processes by three possible ways: (i) opening a double or triple bond, (ii) cleaving a C-C bond, and (iii) by hydrogen abstraction [24, 25].

In order to characterize the active species produced during the proposed atmospheric pressure plasma treatments, optical emission spectroscopy (OES) analysis was performed. Moreover, to verify COOH and NH_2 introduction in the $P_{DL}LA$ 3D scaffold, both treated and untreated samples were characterized by diffuse reflectance infrared spectroscopy (DR-FTIR) using D_2O and NH_3 as probe molecules.

2. Experimental Section

2.1. P (D,L) LA Sponge Preparation. $P_{DL}LA$ (see Figures 1(a) and 1(b), ratio D/L = 1 : 1, average molecular weight 75,000–120,000) was purchased from Sigma-Aldrich (Milwaukee, WI, USA). $P_{DL}LA$ sponge (Figure 1(c)) was prepared by adding $P_{DL}LA$ on chloroform (5% $w_{polymer}/V_{chloroform}$) in 150 mm glass dishes. After one hour of shaking, the solution was casted to plastic dishes and then NaCl (900% $w_{salt}/w_{polymer}$) was spread equally over it. The solvent was evaporated at room temperature overnight. Finally, $P_{DL}LA$ sponges were washed for three days in distilled water to completely remove NaCl.

2.2. Plasma Deposition. The system employed for plasma coating was based on atmospheric plasma pressure dielectric barrier discharge (APP-DBD Platex 600, Grinp S.r.l.) equipped with a stainless steel parallel plate electrode of 800 mm, 230 mm, 35 mm size, providing self-plasma impedance adapting glow discharge [24]. The maximum attainable process power is 2500 W. A rotary pump and a heating chamber were used to vaporize the precursor. The unit was a lab scale roll-to-roll version of an industrial production size system and allowed developing dedicated functionalization processes directly scalable up and transferable to industrial production. The $P_{DL}LA$ substrates were positioned onto a mobile support and very different parameter values were used to perform the two different coatings; in order to avoid the diffusion of the active species from the bottom of the sponges, polypropylene support was used to assure a perfect adhesion of the material to the support. Before the functionalization treatment, all the substrates were activated (using the parameter reported in Table 1) to generate surface radicals that will interact with the plasma species. Helium (He) gas was used as a carrier to introduce the precursor into the plasma region; the precursor concentration used was 0.26 ml min^{-1} for AA (b.p. 139°C) plasma polymerization and 0.30 ml min^{-1} for DAP (b.p. 119.6°C) grafting.

2.3. Diffuse Reflectance Infrared Fourier Transform (DR-FTIR). Infrared spectra were collected on an Equinox 55 Bruker Optics spectrometer with 4 cm^{-1} resolution in the range 4000–600 cm^{-1}. As-prepared materials and after plasma-treated $P_{DL}LA$ sponges were measured in a DR-FTIR cell (Bruker FT-IR Equinox 55 with a diffuse reflectance cell Collector© Spectra-Tech Inc.) equipped with silicon windows permanently attached to a vacuum line (residual pressure < $1^{*}10^{-3}$ mbar) in order to dehydrate all samples under vacuum at room temperature (1 h at 298 K) before the measure. The D_2O adsorption experiments were carried out in situ at 298 K dosing the vapor tension of D_2O (22 mbar) on the samples and successively removing the probe in order to evaluate the proton-deuterium exchange in all materials. In a second time, in another portion of the samples, NH_3 probe molecules were adsorbed: in this case, 50 mbar of NH_3 was put in contact with the samples, and after 30′, the probe molecules were removed progressively and the spectra were recorded at the relative pressure.

2.4. Scanning Electron Microscopy (SEM). SEM images were recorded on a Quanta 200 FEI Scanning Electron Microscope equipped with EDS attachment, using a tungsten filament as electron source. In order to avoid any surface modification, analysis was conducted in low vacuum mode (residual pressure is 110 Pa of H_2O); this residual pressure prevents any electrical charge under the electron beam.

3. Results and Discussion

The main difficulties of a plasma process are connected to the sample morphology (macroporous sponge (Figure 2)) and to the capability of the plasma to uniformly permeate such 3D structure.

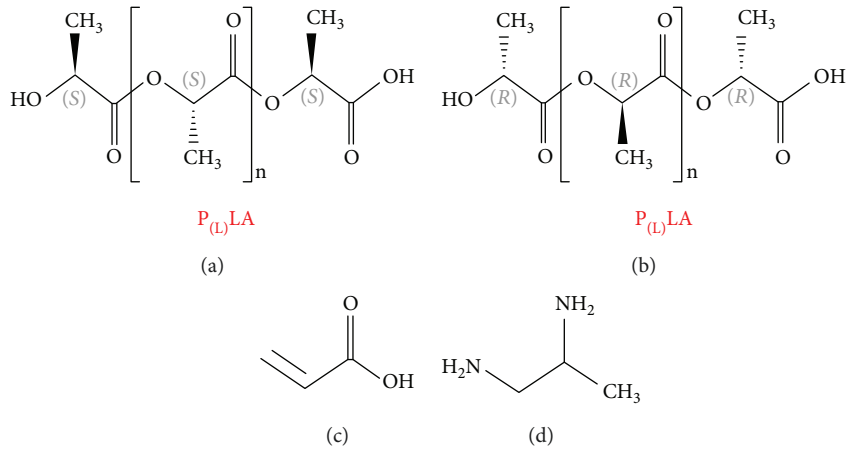

Figure 1: (a, b) Polylactic acid's enantiomorphs; (c) acrylic acid; and (d) 1,2-diaminopropane.

Table 1: Plasma process parameters for continuous and pulsed techniques.

Process description	Gas process	Power (W, (W/cm^2))	Electrode temperature (°C)	Treatment time (s)
Activation	He	240 (0.6)	25	60
Activation	He/O_2	240 (0.6)	25	80
Activation	He/O_2/H_2O	240 (0.6)	25	80
Continuous plasma (-NH_2)	He/DAP	60–120 (0.15-0.3)	50	120
Pulsed plasma (-NH_2)	He/DAP	180–200 (0.45-0.5)	50	180
Continuous plasma (-COOH)	He/AA	60–80 (0.15-0.2)	50	120
Pulsed plasma (-COOH)	He/AA	80–120 (0.2-0.3)	50	180

He gas carries 10 Lmin^{-1}; gas process 0.05 Lmin^{-1}; vaporization temperature in treatments 140°C; pulse parameters: f_{ON} 20, t_{ON} 100, f_{OFF} 100; t_{OFF}.

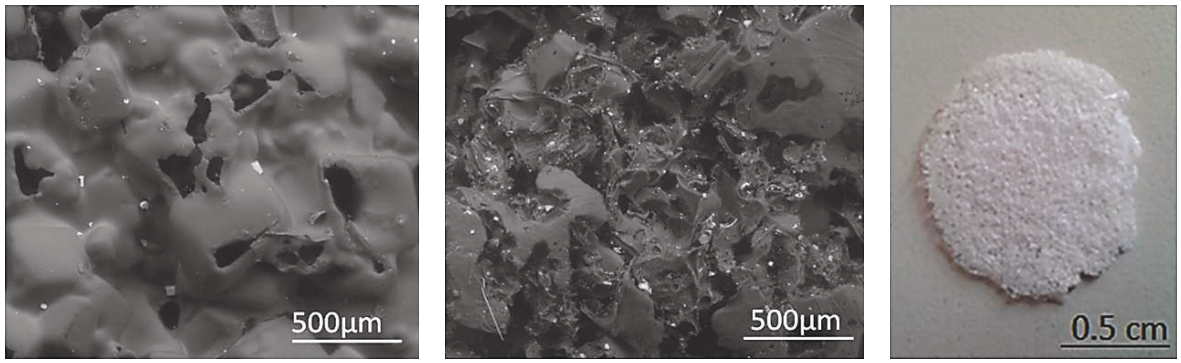

(a) (b) (c)

Figure 2: SEM images show front (a) and back (b) surfaces of nontreated sponge. (c) $P_{(D,L)}LA$ sponge macrophoto.

The studied process consists of two stages: (i) activation of the surface with an oxidant plasma and (ii) deposition of plasma with acrylic acid (pdAA) or DAP on the activated surface.

The first step is required to generate the reactive sites on the $P_{DL}LA$ surface that are essential to firmly link the functionalities during the deposition stage. For this purpose, three activation processes characterized by different oxidative capacities were evaluated: the first one used only He (nonoxidative plasma), the second one a mixture of He and O_2, and the last one a mixture of He, O_2, and sprayed H_2O.

The emissive species generated in these three types of plasma were studied by analysing the OES spectra during the generation of the plasma (Table 2).

The choice of the gas carrier is critical because it is responsible for the energy transfer to reactive species. The most suitable species to this purpose are noble gases, in particular He because of its small size and high

Table 2: Emissive species generated into plasma region evaluated by optical emission spectroscopy.

Species	Wavelength (nm)	Transition
NO γ system	248.34	A $2\Sigma+$ ➔ X 2Π
OH angstrom system	306.45	A $2\Sigma+$ ➔ X 2Π
N_2 second positive system	315.79; 336.76; 357.69; 379.96	C $3\Pi u$ ➔ B $3\Pi g$
CO angstrom series	483.13; 519.67; 561.03	B 1Σ ➔ A 1Π
CO + comet-tail system	427.56	A 2Π ➔ X 2Σ
C_2 swan system	489.08; 516.03	d $3\Pi g$ ➔ a $3\Pi u$
CH	431.24	A 2Δ ➔ X 2Π
H Balmer series	434.47; 485.88; 656.09	$n = 3$ ➔ 2; $n = 4$ ➔ 2; $n = 5$ ➔ 2
H_2	671.74	$d3\Pi - u$ ➔ _a$3\Sigma + g$
He	501; 586; 667; 706	$2s^1S_0$-$3p^1P_1{}^0$; $2P^3p^0{}_{1,2}$–$3d^3D_{1,2,3}$; $2P^1p^0{}_1$–$3d^1D_2$; $2p^3P^0{}_{1,2}$-$3s^3S_1$
O	394.2; 436.77; 615.69; 776.72; 843.8	35P-35S; 33P-33S
O^{2+} system	523.77; 631.43	b4Σ-g ➔ a$4\Pi u$

mobility. As the study was performed using an atmospheric pressure plasma, all the resulting OES spectra also show peaks corresponding to nitrogen and oxygen.

Table 2 shows the typical 501, 586, 667, and 706 nm He peaks [26]. Moreover, N_2 and weaker O_2 emission peaks at 776.72 nm can be identified [28].

Usually, during a plasma process, many competitive mechanisms among surface etching, chain scission, and crosslinking occur as confirmed by the appearance of CH (431.24 nm) and C_2 (489.08; 516.03 nm) peaks after P_{DL}LA scaffold insertion into the plasma region.

When He and O_2 mixture was used, the increase of 776.72 nm signal and the appearance of signals at 843.8 nm (atomic O), 306.45 nm (OH Angstrom system), 483.13, 519.67, and 561.03 nm (CO Angstrom series) were observed.

The emissive species in the third mixture (He, O_2, and H_2O) underwent a considerable intensity decrease of all the signals. The presence of the water molecules resulted in the absorption of a large part of the kinetic energy of the carrier gas. Indeed, from a chemical point of view, there was a reduction of the O radicals confirmed by the disappearance of 843.8 nm signal and the attenuation of the 776.72 nm oxygen signal. On the other hand, there was a significant increase of the signal at 306.45 nm (OH Angstrom system) and at 656.09 nm (H radicals), related to the homolytic cleavage of water molecules.

After the described activation, P_{DL}LA sample surface was modified by gas plasma at atmospheric pressure using DAP (Figure 1(c), 99% pure, Sigma-Aldrich) to add amino groups and acrylic acid (Figure 1(d), 99% pure, Sigma-Aldrich) in order to add carboxylic groups.

After the above described activation process, an organic layer containing carboxylic groups was deposed on the sample surface by both continuous and pulsed plasma treatment. Plasma condition and treatment duration are both related to the energy input into the plasma and transferred to the growing film. For the evaluation of the consequences of different plasma conditions, all the samples were treated for times comprised between 60 and 180 seconds.

Acrylic acid concentration is important because it contributes to determine the thickness of the deposited film and also because it tends to influence the input energy in the plasma and consequentially the amount of energy transferred to the growing film.

During AA deposition, the active species were acquired by OES. AA fragmentation was monitored through OH (306.45 nm) signal in function of the power and the plasma modality (continuous or pulsed) [29].

In order to increase the functionalization and the stability of the deposited film, pulsed plasma method was introduced by Yasuda [30]; in this modality, a time frame both for active and inactive plasma is applied.

During the ignition time, the breaking of the precursor molecules, the formation of the reactive species, and the consequent polymerization reactions occur. In the second time, the radical chain previously formed spreads keeping the typical precursor functional groups allowing chemical reaction processes rather than those with pure or predominant dissociation generated by plasma.

The main parameters of this method are the pulse time and the duty cycle (DC), defined as

$$\mathrm{DC} = \frac{t_{\mathrm{on}}}{(t_{\mathrm{on}} + t_{\mathrm{off}})}, \tag{1}$$

which is the fraction of the plasma ignition time compared to the complete duration of the pulse time ($t_{\mathrm{on}} + t_{\mathrm{off}}$).

In pulsed plasma conditions, the reactive species that are generated during the activation time t_{on} are consumed during the switch-off time t_{off}.

Usually, the more reactive species are readily consumed during the initial moment of the switch-off, and at the same time, the competitive processes involving radical-radical recombination decrease along the increasing of t_{off} time, allowing the radical-monomer reactions. Furthermore, both photochemical reactions and substrate overheating are controlled in pulsed plasma modality, which allow to have a selective mechanism of the reaction on the substrates.

In particular, during the AA polymerization in pulsed plasma mode, it is possible to act selectively on the π bond, inducing the homolytic break with the formation of radicals

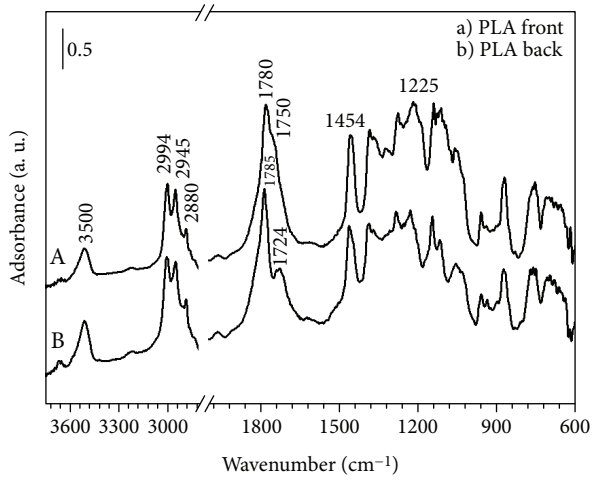

FIGURE 3: DR-FTIR spectra in the range 3700–700 cm^{-1} of (a) "front" and (b) back of $P_{DL}LA$ sponges.

available for the polymerization reaction. These reactions occur during the t_{off} time, leading to film with high density of carboxylic groups (low fragmentation conditions).

In the pulsed glow discharge, the poisoning effect of oxygen-containing group is also reduced due to the low duty cycle of the pulse, but once formed, the radicals can be conserved by the vinyl double bond during the "off" period.

The final effects of a pulsed radio frequency discharge on acrylic acid are the following:

(1) Remarkable increase in the polymer deposition rate

(2) Increase in the concentration of free radicals trapped in the plasma polymer

(3) Decrease in the substrate $P_{DL}LA$ signals

(4) Significant increase in the wettability by water of the plasma polymer

The polymer formation from this monomer depends heavily on cycle II (diradicals) [30].

All processes were characterized using probe molecules in DR-FTIR spectroscopy in order to obtain information about the effective efficiency of the different treatments.

3.1. DR-FTIR Analysis

3.1.1. Plasma Treatment. $P_{DL}LA$ sponges are 3D structures, with a side directly exposed to plasma treatment (front) and a side not directly exposed to plasma (back). To evaluate the permeability and the diffusion of plasma treatment across the macroporous structure, the back side of the sponges was analysed along with the front to estimate the plasma process efficiency.

DR-FTIR characterization was performed by adsorption of probe molecules such as deuterated water (D_2O) and ammonia (NH_3). D_2O molecule was used to assign the spectral components related to the presence of OH and –NH groups, as hydrogen can exchange with deuterium to form –OD or -ND groups. On the other hand, the use of ammonia on carboxylic functionalities can lead to acid-base interactions with the subsequent formation of the ammonium ion, showing characteristic IR bands.

Before discussing the changes after the interaction of probe molecules and the functionalized $P_{DL}LA$, a short assignment of spectrum of $P_{DL}LA$ was reported. As it can be seen from Figure 3, $P_{DL}LA$ polymer is mainly characterized by the presence of $-CH_3$, -CH, -C=O, and -COC- groups that form the framework and -OH group in the terminal of the polymer chain.

Figure 3 shows the DR-FTIR spectra of the $P_{DL}LA$ sponge on the front (a) and on the back (b).

The front of the $P_{DL}LA$ sponge reported in Figure 3(a) shows at high-frequency region a band at 3500 cm^{-1} due to free -OH stretching and in the 3000–2800 cm^{-1} region $-CH_3$/-CH stretching modes, while at low frequencies, the strong band at about 1780 cm^{-1} with a shoulder at 1750 cm^{-1} is attributable to the -C=O stretching, as a broad asymmetric band mainly due to A and E1 active modes. In the low-frequency region, at 1454 cm^{-1} due to the bending of $-CH_3$ group, while at 1225 cm^{-1} attributed to ether group.

The spectrum of the back of the sponge (Figure 3(b)) shows similar bands to the spectra of the front; the main difference is related to the band at 1780 cm^{-1} which is shifted at 1785 cm^{-1} with a more evident shoulder which appears at about 1724 cm^{-1}. The origin of spectral splitting, showed also in the front, is still not well interpreted; some theories in literature attribute it to the intramolecular coupling or interchain interactions which depends on the structural changes taking place during melt/crystallization. [31, 32].

3.2. Continuous and Pulsed Plasma – COOH Functionalizations

3.2.1. Dosage of D_2O Probe Molecules. In Figure 4, the spectra of the front and back of $P_{DL}LA$ functionalized with -COOH before and after contact with D_2O are reported, respectively. The curves in Figure 4(a) refer to the spectra of sample before D_2O adsorption and the curves in Figure 4(b) are the spectra of the sample in vacuum after the interaction with 22 mbar (vapor pressure at 25°C) of D_2O ($P < 1 * 10^{-2}$ mbar). In order to obtain a complete exchange of –H with –D species, the adsorption and desorption of D_2O were repeated three times.

Figures 4(a) and 4(b) are reported spectra of samples functionalized with –COOH by continuous plasma (front and back, respectively), and Figures 4(c) and 4(d) are samples functionalized with –COOH by pulsed plasma (front and back, respectively).

In Figure 4(a)–4(d), it is possible to observe the presence of a new broad band in the region between 2800 and 2100 cm^{-1} with different overlaid components.

As reported in literature [33], pure D_2O is characterized by asymmetric, symmetric, and bending vibration modes; in the case of partial exchange, HOD species are also present. D_2O asymmetric, symmetric stretching modes, and the bending first overtone are characterized by broad absorption band in the region 2300–2700 cm^{-1}, with maximum at 2621

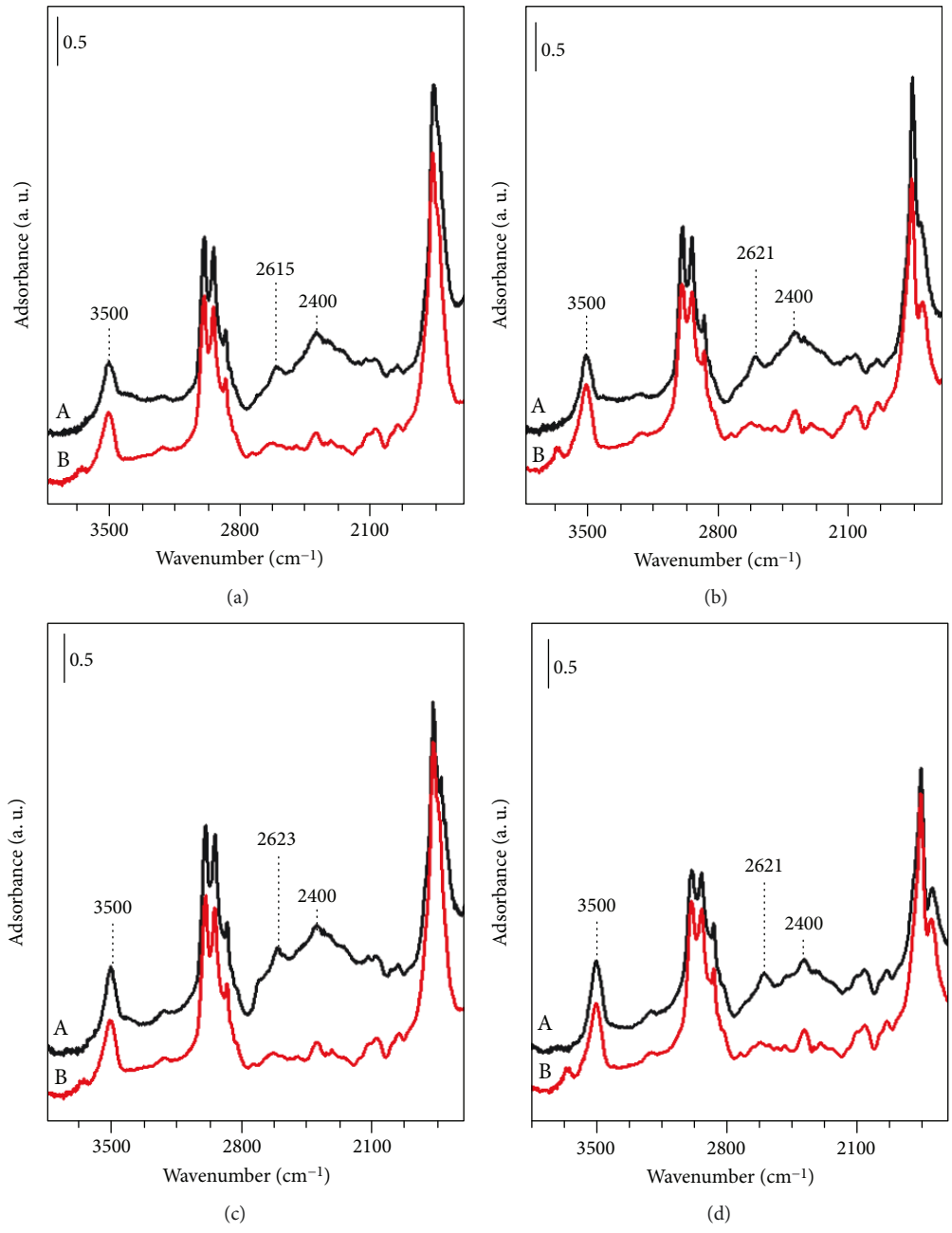

Figure 4: DR-FTIR spectra in the range 3700–1600 cm^{-1} of (a) spectra of samples in vacuum; (b) spectra of samples in vacuum after the interaction with $D_2O_{(g)}$.

and 2400 cm^{-1}. While for HOD species, the OH and OD stretches are well separated in narrow bands: OD stretch at 2500 cm^{-1} and OH stretch at 3500 cm^{-1}. The bands of D_2O and HOD may undergo shifts due to the effects of weak and strong hydrogen bonding.

The plasma treatments can introduce new components in the spectra related to additional –OH groups derived after the fragmentation of the polymer chain.

Since the region 3700–1800 cm^{-1} is characterized by structural bands, to see the difference before and after OH-OD exchange, it is better to consider subtracted spectra shown in Figure 5, obtained by subtracting the starting curves from those after the interaction with D_2O.

In Figures 5(a) and 5(b), the subtracted spectra of the treated samples are shown in the front and in the back, respectively. The first perturbation is observed at 3600–3500 cm^{-1} which is attributed to terminal –OH groups which undergoes a partial HOD exchange: in particular, the negative component at 3550 cm^{-1} and the broad negative band centred at about 3250 cm^{-1} undergo deuterium exchange in both plasma-treated samples, demonstrated by the positive band with low intensity centred at about 2600 cm^{-1}. The shoulder at 2700 cm^{-1} is due to D_2O bending first overtone mode. New positive broad band also appeared in the region 2550–1800 cm^{-1} centred at 2370 cm^{-1}, attributed to asymmetric and symmetric D_2O stretch.

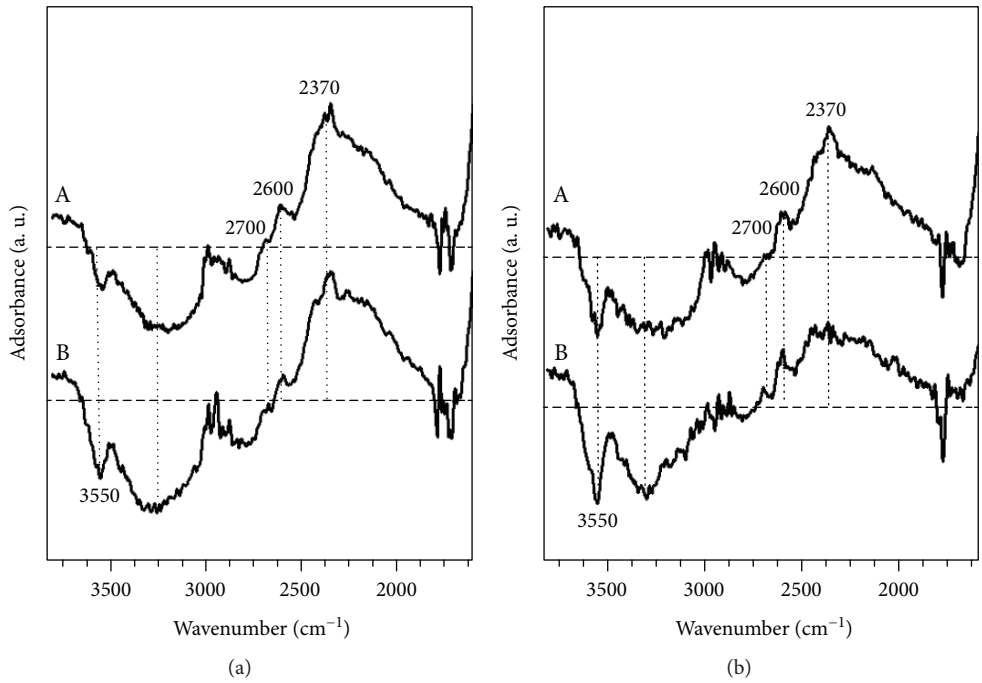

Figure 5: DR-FTIR subtraction spectra in the range 3700–1800 cm^{-1} of outgassed samples after interaction with $D_2O_{(g)}$. (a) $P_{(D,L)}$LA-COOH treated by continuous plasma (front of the sponges) and (b) $P_{(D,L)}$LA-COOH treated by pulsed plasma (back of the sponges).

The relative intensity of these components is similar in both continuous and pulsed plasma-treated "front" samples, while in the "back," the pulsed plasma-treated sample is characterized by lower band intensity. This behaviour confirms a lower surface damage with pulsed plasma.

3.2.2. Dosage of NH_3 Probe Molecules. To evaluate the effective success of the –COOH functionalization by plasma treatments, NH_3 adsorption on materials was done; in this case, an acid-base reaction between NH_3 and the acidic functional groups of the material is observed. The corresponding spectra are shown in Figure 6.

After adsorption of NH_3, the spectra, reported in Figure 6(a)–6(d), show change in the intensities of the components at about 3200 and 1590 cm^{-1}.

The adsorption of ammonia on polymeric materials gives different bands due to its interaction with functionalities on the surface: in the case of P_{DL}LA, it can be found in the high-frequency region mainly stretching vibrations of free –NH and –OH groups, while in the low-frequency region, NH^{4+} bending modes derived by the acid-base interaction between ammonia and –COOH or –OH functionalities, and finally vibration modes of $–COO^-$ groups.

Also in this case, in order to better highlight changes between samples before and after the adsorption of NH_3, it is possible to evaluate the subtracted spectra, shown in Figure 7.

In Figure 7(a), at high-frequency region, broad bands at about 3100 and 2800 cm^{-1} are attributed to –NH stretching of hydrogen-bonded NH groups. At the back of the sponge reported in Figure 7(b), additional bands are shown for the samples treated by pulsed plasma at 3420 cm^{-1} and 3260 cm^{-1}, which can be assigned to NH groups not involved in hydrogen bonding [34]. In the low-frequency region, the interaction of ammonia with Brønsted acid sites and the formation of ammonium salts of carboxylic acid are demonstrated. IR spectra show a broad band at 1585 cm^{-1} and 1360 cm^{-1} due to asymmetric and symmetric COO^- group, beside the ammonium ion bending (NH^{4+}) at about 1420 cm^{-1} [35].

The intensity of these bands is similar at the front for continuous and pulsed plasma-treated samples, which indicates a similar efficiency of functionalization on the front, while at the back of the sponges, the bands are more intense in the pulsed plasma-treated sample, which indicate higher efficiency of functionalization pulsed mode plasma in the 3D structure.

3.3. Continuous and Pulsed Plasma –NH_2 Functionalizations

3.3.1. Dosage of D_2O Probe Molecules. As already reported in the sample treated with acrylic acid, also for the plasma treatments with DAP precursor, the effectiveness and uniformity of the plasma treatments through the adsorption of probe molecules have been studied; in particular, adsorption of deuterated water was used to evaluate the presence of –NH groups, which can exchange in –ND.

In Figure 8, the subtracted spectra of the front and back of P_{DL}LA functionalized with $–NH_2$ before and after contact with D_2O are reported.

The spectra of the front of the sponges (Figure 8(a)) show two distinct regions: the first, between 3400 cm^{-1} and 2700 cm^{-1}, shows the presence of bands that disappeared, mainly associated to free NH_2 groups or bound as $RCONH_2$ and to free structural OH groups derived from terminal

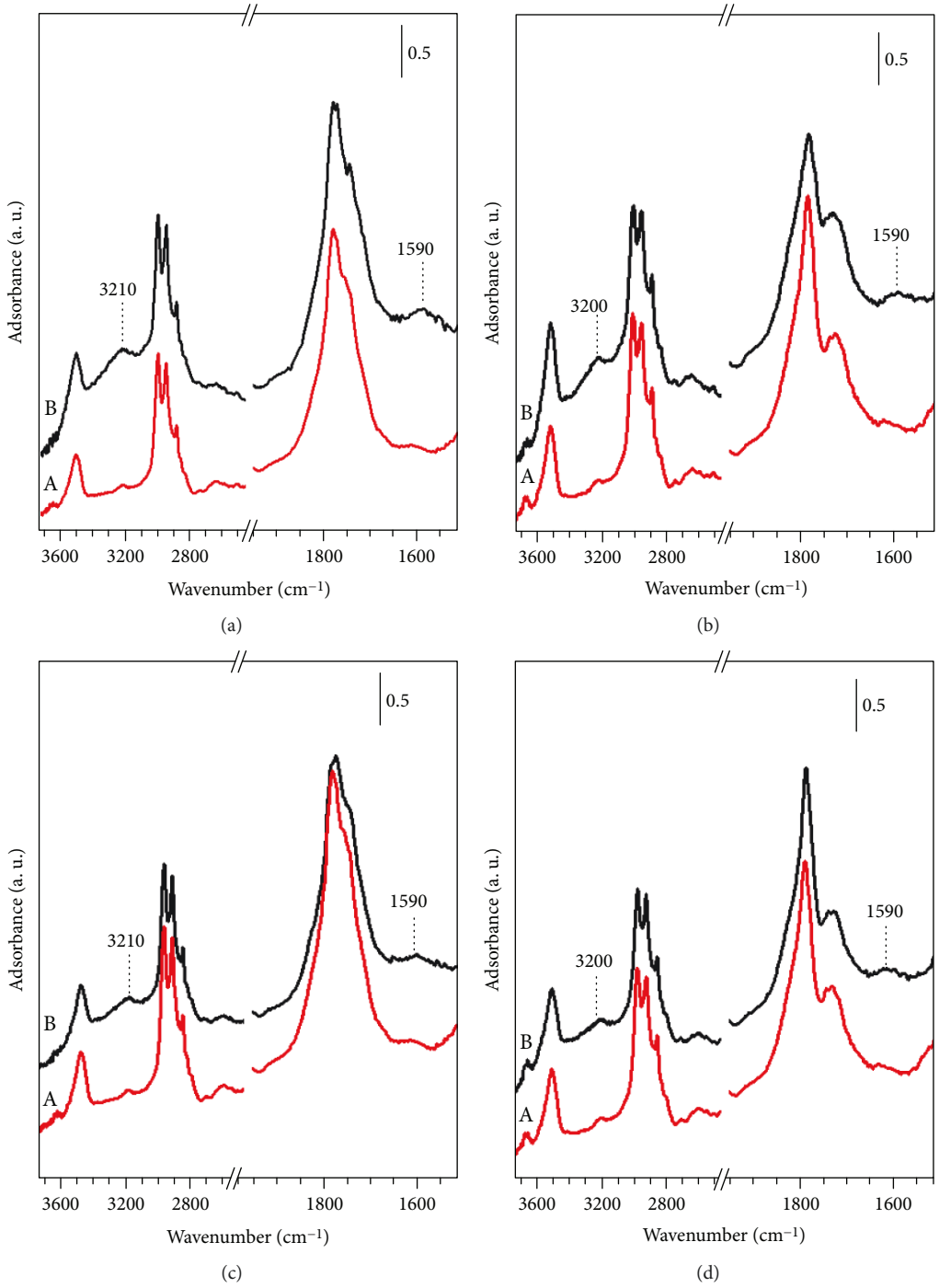

FIGURE 6: DR-FTIR spectra in the range 3700–1600 cm^{-1} of (a) spectra of sample in vacuum; (b) spectra of sample in vacuum after the interaction with $NH_{3(g)}$. (a, b) Spectra of samples functionalized with –COOH by continuous plasma (front and back, respectively). (c, d) Samples functionalized with –COOH by pulsed plasma (front and back, respectively).

groups of the polymer. Consequently, in the second part, new broad bands with different overlapped components appeared in the region 2700–2000 cm^{-1}.

After plasma $-NH_2$ functionalization treatment, the negative component at 3200 cm^{-1} undergoes deuterium exchange in both plasma-treated samples. The new positive broad bands with the maximum at 2445 and 2475 cm^{-1} are attributed mainly to ND stretch bands [36].

The back confirms the behaviour shown in the front with a little shift to 2480 and 2240 cm^{-1} (Figure 8(b)) and confirms a higher surface $-NH_2$ functionalization with pulsed plasma.

3.3.2. Continuous and Pulsed Plasma Morphology. Sponge morphology after continuous and pulsed plasma treatment has been also considered. As shown in Figure 9, the

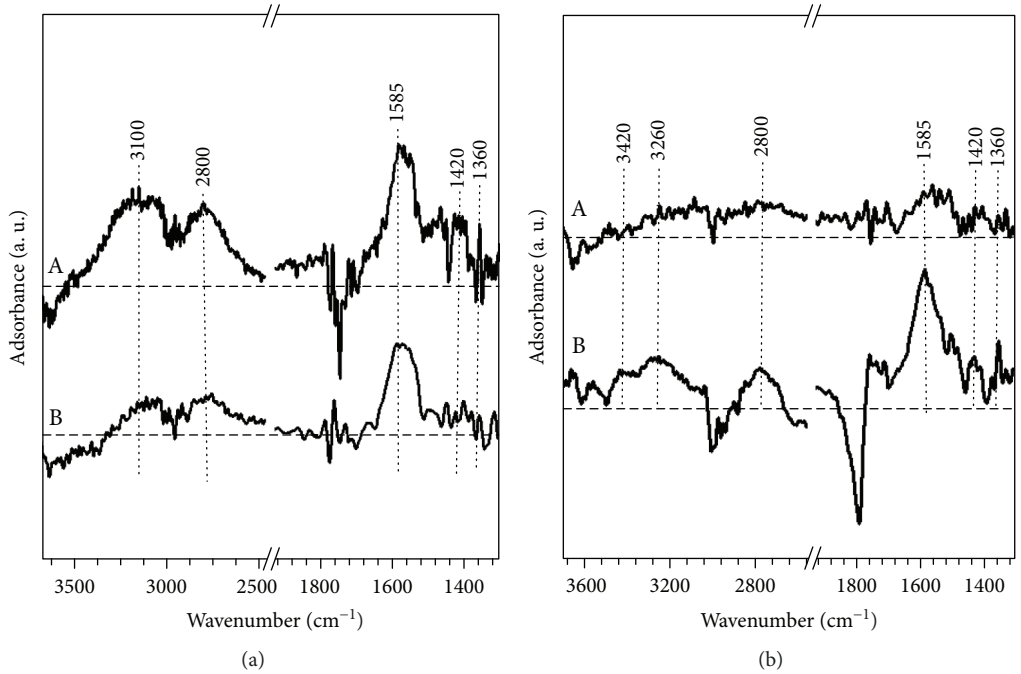

Figure 7: DR-FTIR subtraction spectra in the range 3700–1300 cm^{-1} of outgassed samples at 10^{-2} mbar after interaction with $NH_{3(g)}$. (a) $P_{(D,L)}LA$ treated with continuous plasma (front) and (b) $P_{(D,L)}LA$ treated with pulsed plasma (back).

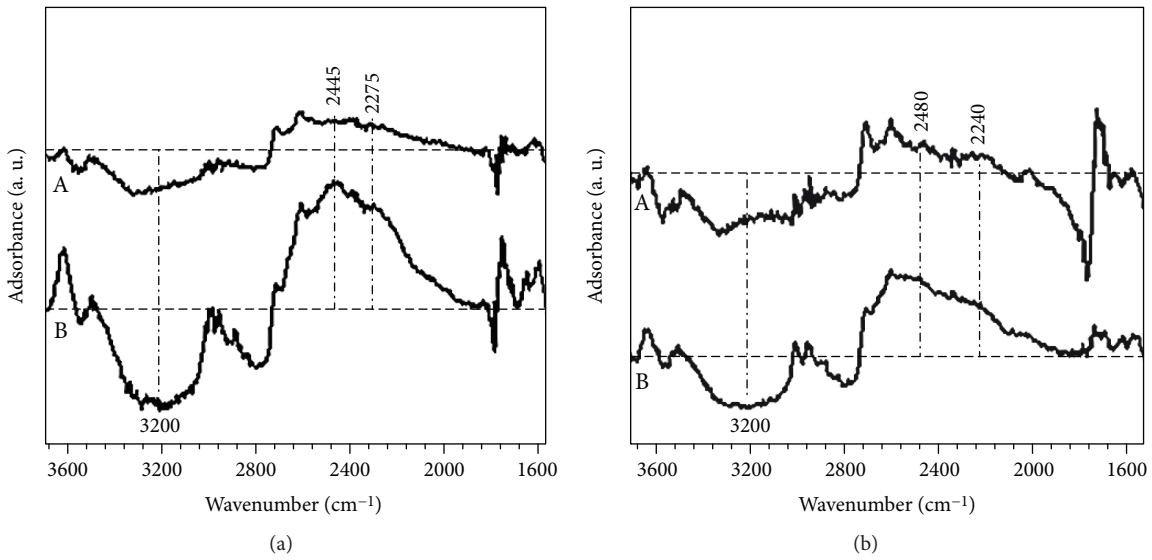

Figure 8: DR-FTIR subtraction spectra in the range 3700–1550 cm^{-1} of outgassed samples after interaction with $D_2O_{(g)}$. (a) $P_{(D,L)}LA$ continuous plasma treated (front) and (b) $P_{(D,L)}LA$ pulsed plasma treated (back) with $-NH_2$ functionality.

morphology of the front part of the sponges was altered compared to the untreated (CT) samples. In particular, the continuous plasma treatment seemed to obliterate the majority of matrix pores, while pulsed plasma treatment was able to reduce the pore areas giving a smoother aspect to the matrix front surface compared to CT samples. The effect observed in the samples treated with continuous plasma could be caused by the higher energy used compared to pulsed treatment. Furthermore, the matrix back part showed a similar morphology in all samples treated or untreated.

4. Conclusions

The functionalization of 3D $P_{DL}LA$ sponges using atmospheric plasma both in continuous and pulsed mode has been studied in this paper. Characterization of the species produced during plasma processes was performed by optical emission spectroscopy (OES). The effects of the continuous and pulsed mode on the functionalization of the $P_{DL}LA$ surface were investigated. In the case of acrylic acid deposition with plasma pulsed technique, there are combined effects of

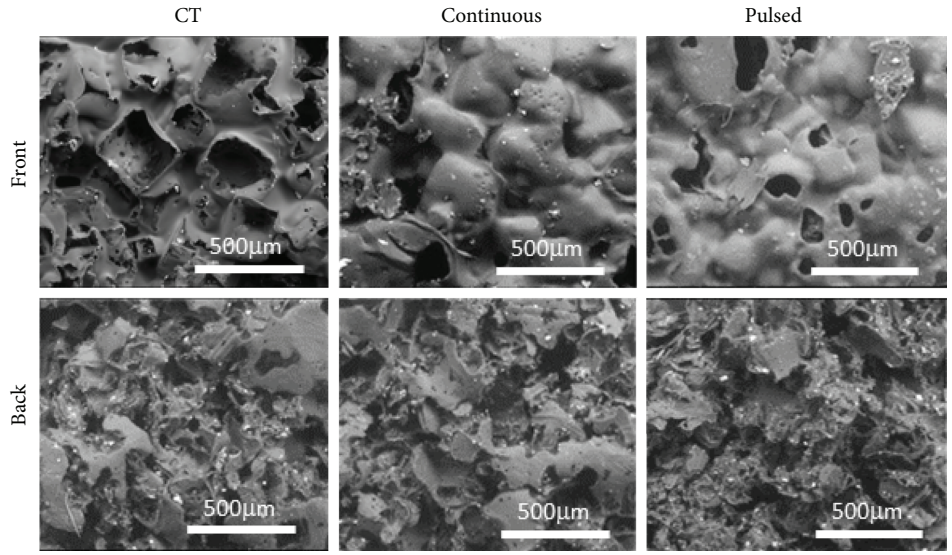

Figure 9: SEM images for untreated (CT) and plasma-treated samples.

low power and small duty cycle which allow at the same time better growth of acrylic acid thin film and the retention of –COOH groups. The concentration of C=O species, investigated with OES, is used as marker to optimize the –COOH functionalization [37]. Also, in the case of DAP, the deposition with pulsed mode was more efficient. This suggests that in these conditions the amine functionalities are retained to a greater extent than in the continuous mode.

The $P_{DL}LA$ sponges after the –COOH and $–NH_2$ functionalization treatments were characterized by FTIR spectroscopy, using the diffuse reflectance technique (DR-FTIR). With this technique, the samples were measured after adsorption of probe molecules (D_2O and NH_3) to assess the type of functional groups incorporated with the plasma treatment.

IR spectra after D_2O and NH_3 addition showed an increase in -OH -COOH and $-NH_2$ functional groups exposed by both pulsed plasma- and continuous plasma-treated surfaces.

Continuous plasma treatment, using high power, modified the matrix front part morphology, increased polymer chain fragmentation, resulting in a large number of free -OH terminal groups, while the pulsed plasma treatment showed a more efficient grafting of both carboxyl and amine functional groups, associated with higher permeability with low structural damages.

Finally, the continuous treatment is most effective on the part processed directly, while the pulsed plasma is able to provide a more homogeneous result, also in the thickness of the sample, showing that the interior of the 3D porous scaffold undergoes functionalization.

Data Availability

The data used to support the findings of this study are available from the corresponding author upon request.

Conflicts of Interest

The authors declare that there is no conflict of interest regarding the publication of this paper.

Acknowledgments

The financial support by Finpiemonte (2014) (code ASF 284-30C) is gratefully acknowledged.

References

[1] A. G. Andreopoulos, E. Hatzi, M. Doxastakis, and J. Mater, "Synthesis and properties," *Journal of Materials Science: Materials in Medicine*, vol. 10, pp. 29–33, 1999.

[2] R. E. Drumright, P. R. Gruber, and D. E. Henton, "Polylactic acid technology," *Advanced Materials*, vol. 12, no. 23, pp. 1841–1846, 2000.

[3] C. M. Agrawal, J. Best, J. D. Heckman, and B. D. Boyan, "Protein release kinetics of a biodegradable implant for fracture non-unions," *Biomaterials*, vol. 16, no. 16, pp. 1255–1260, 1995.

[4] J. Slager and A. J. Domb, "Biopolymer stereocomplexes," *Advanced Drug Delivery Reviews*, vol. 55, no. 4, pp. 549–583, 2003.

[5] R. Morent, N. De Geyter, M. Trentesaux et al., "Influence of discharge atmosphere on the ageing behaviour of plasma-treated polylactic acid," *Plasma Chemistry and Plasma Processing*, vol. 30, no. 4, pp. 525–536, 2010.

[6] C. Oehr, "Plasma surface modification of polymers for biomedical use," *Nuclear Instruments and Methods in Physics Research Section B: Beam Interactions with Materials and Atoms*, vol. 208, pp. 40–47, 2003.

[7] P. K. Chu, J. Y. Chen, L. P. Wang, and N. Huang, "Plasma-surface modification of biomaterials," *Materials Science and Engineering: R: Reports*, vol. 36, no. 5-6, pp. 143–206, 2002.

[8] J. M. Morais, F. Papadimitrakopoulos, and D. J. Burgess, "Biomaterials/tissue interactions: possible solutions to overcome foreign body response," *AAPS Journal*, vol. 12, pp. 188–196, 2010.

[9] B. D. Ratner, "The engineering of biomaterials exhibiting recognition and specificity," *Journal of Molecular Recognition*, vol. 9, no. 5-6, pp. 617–625, 1996.

[10] R. Forch, Z. Zhang, and W. Knoll, "Soft plasma treated surfaces: tailoring of structure and properties for biomaterial applications," *Plasma Processes and Polymers*, vol. 2, no. 5, pp. 351–372, 2005.

[11] A. Jordá-Vilaplana, V. Fombuena, D. García-García, M. D. Samper, and L. Sánchez-Nácher, "Surface modification of polylactic acid (PLA) by air atmospheric plasma treatment," *European Polymer Journal*, vol. 58, pp. 23–33, 2014.

[12] J. A. Neff, P. A. Tresco, and K. D. Caldwell, "Surface modification for controlled studies of cell–ligand interactions," *Biomaterials*, vol. 20, no. 23-24, pp. 2377–2393, 1999.

[13] R. H. Hansen, J. V. Pascale, T. DeBenedectis, and P. M. Rentzepis, "Effect of atomic oxygen on polymers," *Journal of Polymer Science Part A: General Papers*, vol. 3, no. 6, pp. 2205–2214, 1965.

[14] D. T. Clark and A. Dilks, "ESCA applied to polymers. XVIII. RF glow discharge modification of polymers in helium, neon, argon, and krypton," *Journal of Polymer Science: Polymer Chemistry Edition*, vol. 16, no. 5, pp. 911–936, 1978.

[15] V. Kudryavtseva, K. Stankevich, A. Gudima, E. Kibler, and S. Tverdokhlebov, "Atmospheric pressure plasma assisted immobilization of hyaluronic acid on tissue engineering PLA-based scaffolds and its effect on primary human macrophages," *Materials & Design*, vol. 127, pp. 261–271, 2017.

[16] S. O'Kell, T. Henshaw, G. Farrow, and C. Jones, "Effects of low-power plasma treatment on polyethylene surfaces," *Surface and Interface Analysis*, vol. 23, no. 5, pp. 319–327, 1995.

[17] S. Pringle, V. Joss, and C. Jones, "Ammonia plasma Treatment of PTFE under known plasma conditions," *Surface and Interface Analysis*, vol. 24, no. 12, pp. 821–829, 1996.

[18] L. Detomaso, R. Gristina, G. S. Senesi, R. d'Agostino, and P. Favia, "Stable plasma-deposited acrylic acid surfaces for cell culture applications," *Biomaterials*, vol. 26, no. 18, pp. 3831–3841, 2005.

[19] C. Oehr, M. Muller, B. Elkin, D. Hegemann, and U. Vohrer, "Plasma grafting — a method to obtain monofunctional surfaces," *Surface and Coatings Technology*, vol. 116-119, pp. 25–35, 1999.

[20] Z. Ma, C. Gao, Y. Gong, and J. Shen, "Chondrocyte behaviors on poly-l-lactic acid (PLLA) membranes containing hydroxyl, amide or carboxyl groups," *Biomaterials*, vol. 24, no. 21, pp. 3725–3730, 2003.

[21] D. B. Haddow, S. McNeil, and R. D. Short, "A cell therapy for chronic wounds based upon a plasma polymer delivery surface," *Plasma Processes and Polymers*, vol. 3, no. 6-7, pp. 419–430, 2006.

[22] A. D. Hanson, M. Wall, B. Pourdeyhimi, and E. G. Loboa, "Effects of oxygen plasma treatment on adipose-derived human mesenchymal stem cell adherence to poly(L-lactic acid) scaffolds," *Journal of Biomaterials Science, Polymer Edition*, vol. 18, no. 11, pp. 1387–1400, 2007.

[23] C. M. Alves, Y. Yang, D. L. Carnes et al., "Modulating bone cells response onto starch-based biomaterials by surface plasma treatment and protein adsorption," *Biomaterials*, vol. 28, no. 2, pp. 307–315, 2007.

[24] J. L. Polan, B. Morse, S. Wetherold et al., "VEGF analysis induced by endothelialized gas-plasma treated d,l-PLA scaffolds," *Cardiovascular Radiation Medicine*, vol. 3, no. 3-4, pp. 176–182, 2002.

[25] J. H. Lee, G. Khang, J. W. Lee, and H. B. Lee, "Interaction of different types of cells on polymer surfaces with wettability gradient," *Journal of Colloid and Interface Science*, vol. 205, no. 2, pp. 323–330, 1998.

[26] F. Renò, D. D'Angelo, G. Gottardi et al., "Atmospheric pressure plasma surface modification of poly(D,L-lactic acid) increases fibroblast, osteoblast and keratinocyte adhesion and proliferation," *Plasma Process and Polymers*, vol. 9, no. 5, pp. 491–502, 2012.

[27] M. Wang, P. Favi, X. Cheng et al., "Cold atmospheric plasma (CAP) surface nanomodified 3D printed polylactic acid (PLA) scaffolds for bone regeneration," *Acta Biomaterialia*, vol. 46, pp. 256–265, 2016.

[28] C. Lee, M. Yi, and G. Y. Chung, "Characteristics of He/O_2 atmospheric pressure glow discharge and its dry etching properties of organic materials," *Surface and Coating Technology*, vol. 146-147, pp. 474–479, 2001.

[29] O. Carton, D. Ben Salem, S. Bhatt, J. Pulpytel, and F. Arefi-Khonsari, "Plasma polymerization of acrylic acid by atmospheric pressure nitrogen plasma jet for biomedical applications," *Plasma Processes and Polymers*, vol. 9, no. 10, pp. 984–993, 2012.

[30] H. Yasuda, *Plasma Polymerization*, Academic Press Inc., Orlando, FL, USA, 1985.

[31] E. Meaurio, E. Zuza, N. Lopez-Rodriguez, and J. R. Sarasua, "Conformational behavior of poly(l-lactide) studied by infrared spectroscopy," *The Journal of Physical Chemistry B*, vol. 110, no. 11, pp. 5790–5800, 2006.

[32] J. R. Sarasua, N. L. Rodriguez, A. L. Arraiza, and E. Meaurio, "Stereoselective crystallization and specific interactions in polylactides," *Macromolecules*, vol. 38, no. 20, pp. 8362–8371, 2005.

[33] J. C. Deàk, S. T. Rhea, L. K. Iwaki, and D. D. Dlott, "Vibrational energy relaxation and spectral diffusion in water and deuterated water," *The Journal of Physical Chemistry A*, vol. 104, no. 21, pp. 4866–4875, 2000.

[34] A. Zecchina, L. Marchese, S. Bordiga, C. Pazé, and E. Gianotti, "Vibrational spectroscopy of NH_4^+ ions in zeolitic materials: an IR study," *The Journal of Physical Chemistry B*, vol. 101, no. 48, pp. 10128–10135, 1997.

[35] J. Zawadzki, M. Wiśniewski, and K. Skowrońska, "In situ characterization of interaction of ammonia with carbon surface in oxygen atmosphere," *Carbon*, vol. 41, no. 12, pp. 2257–2267, 2003.

[36] N. S. Murthy, M. Stamm, J. P. Sibilia, and S. Krimm, "Structural changes accompanying hydration in nylon 6," *Macromolecules*, vol. 22, no. 3, pp. 1261–1267, 1989.

[37] F. Palumbo, P. Favia, A. Rinaldi, M. Vulpio, and R. D'Agostino, "PE-CVD of organic thin films with controlled surface concentration of carboxylic groups," *Plasmas and Polymers*, vol. 4, no. 2-3, pp. 133–145, 1999.